Biophysical Journal, Volume 97

Supporting Material

Combining laser microsurgery and finite element modeling to assess cell-level epithelial mechanics

M. Shane Hutson, Jim Veldhuis, Xiaoyan Ma, Holley E. Lynch, P. Graham Cranston, and G. Wayne Brodland

SUPPORTING MATERIAL

Note S1: Correlations with the local cell geometry. The FE model yields a wide range of recoil velocities – even when results are limited to a single angle with a specific set of boundary conditions. This wide range occurs despite a uniform viscosity and uniform cell-edge tensions. It is instead caused by local differences in cell geometry. To illustrate the geometric influences, we present a local approximation to the full finite element matrix equation. For a node at the end of a wounded edge (e.g. node A in Fig 1 of the main text), one can write an equation of dynamic equilibrium with respect to the edge direction (x'):

$$(\eta_{1xx} + \eta_{2xx} + \eta_{3xx})\mathrm{v}_{x0} \approx \gamma(\cos\alpha + \cos\varepsilon) + \langle\sigma_{in}\rangle\delta(d_{AC}\sin\alpha + d_{AE}\sin\varepsilon)/2 \qquad \text{Eqn S1.}$$

The right-hand side is the post-ablation force imbalance at node A due to tension along the two non-ablated edges and the internal stress in cell #3 (approximated by the average internal stress). The geometric parameters are defined in Fig 1 of the main text. The left-hand side is a viscous force where η_{mxx} is the effective drag coefficient for motion along x' due to cell m. For each cell, the drag coefficient is calculated on the basis of two orthogonal systems of dashpots (1). These dashpot systems define a 2×2 damping matrix in the cell's principle coordinate system

$$\boldsymbol{\eta} = \frac{4\pi a\delta\mu}{n}\begin{bmatrix}\sqrt{I_{\min}/I_{\max}} & 0\\ 0 & \sqrt{I_{\max}/I_{\min}}\end{bmatrix} \qquad \text{Eqn S2}$$

where $a = 0.682$ is an empirical constant, n is the number of nodes in the cell and $I_{\min}$ and $I_{\max}$ are the cell's principle moments of inertia. To find η_{mxx}, the damping matrix is rotated into the frame of the ablated edge ($R^{\mathrm{T}}\eta R$). A primary impact of Eqn S2 is to make η_{nxx} smaller when a cell is extended along x'. For Eqn S1, we take the first order approximation in which only node A moves and only in the x'-direction.

Eqn S1 can be recast in dimensionless parameters as:

$$G_{xx}\nu_0 \approx C_\gamma + \langle\Sigma_{in}\rangle C_\Sigma \qquad \text{where} \quad G_{xx} = (\eta_{1xx} + \eta_{2xx} + \eta_{3xx})/(2\mu\delta) \qquad \text{Eqn S3}$$

$$C_\gamma = \cos\alpha + \cos\varepsilon$$

$$C_\Sigma = (\chi_{AC}\sin\alpha + \chi_{AE}\sin\varepsilon)/4$$

G_{xx}, C_γ and C_Σ respectively capture the influence of cell geometry on viscous damping, the imbalance of cell-edge tensions and the imbalance of internal cell stress. ν_0 always increases with C_γ and decreases with G_{xx} (Fig S1). Both dependencies reflect increases in ν_0 as cells become more elongated in the direction parallel to the ablated edge – which decreases each η_{nxx} and makes the triple-junction angles more acute. The dependence of ν_0 on C_Σ is much weaker, and is not readily apparent until one includes the viscous damping effects (Fig S1, ν_0 versus C_Σ / G_{xx}). When all three effects are included, the local approximation accounts for 50-60% of the variance in ν_0.

The variation in G_{xx} has a critical influence on recoil velocity that is often overlooked. For example, Rauzi et al modeled the geometry dependence of ν_0 based solely on the imbalance of cell edge tensions in an idealized geometry of stretched hexagonal cells (2). They assumed uniform viscous damping that canceled out of ν_0 comparisons. Although they attributed

differences between model and experiments to cell-edge elasticity, we estimate that G_{xx} should actually decrease by a factor of $\sqrt{3}$ over the range of cell shapes considered – accounting for roughly half of their observed differences.

1. Brodland, G. W., D. Viens, and J. H. Veldhuis. 2007. A new cell-based FE model for the mechanics of embryonic epithelia. Comp. Meth. Biomech. Biomed. Engr. 10:121-128.
2. Rauzi, M., P. Verant, T. Lecuit, and P. F. Lenne. 2008. Nature and anisotropy of cortical forces orienting Drosophila tissue morphogenesis. Nature Cell Biology 10:1401-1410.

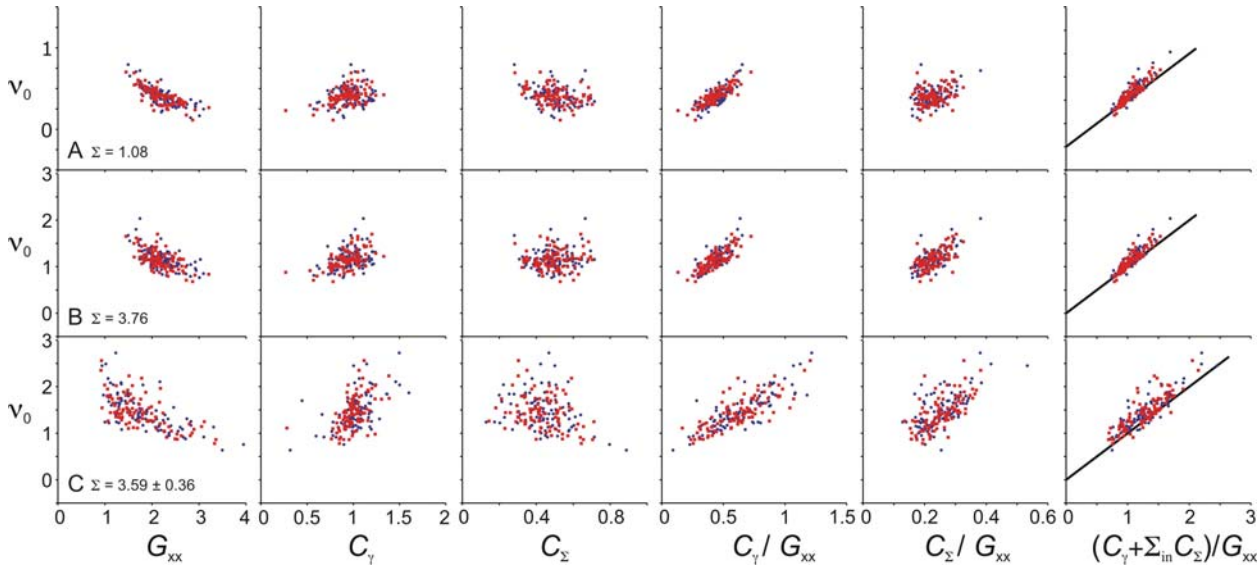

FIGURE S1. Correlations between the recoil velocity and local cell geometry. Each row of graphs corresponds to a different far-field stress (as noted). The geometric factors G_{xx}, C_γ and C_Σ are defined in Eqn S3. The last plot on each row compares the simulated v_0 to that predicted based on Eqn S3 and the local cell geometry (solid line is $y = x$).

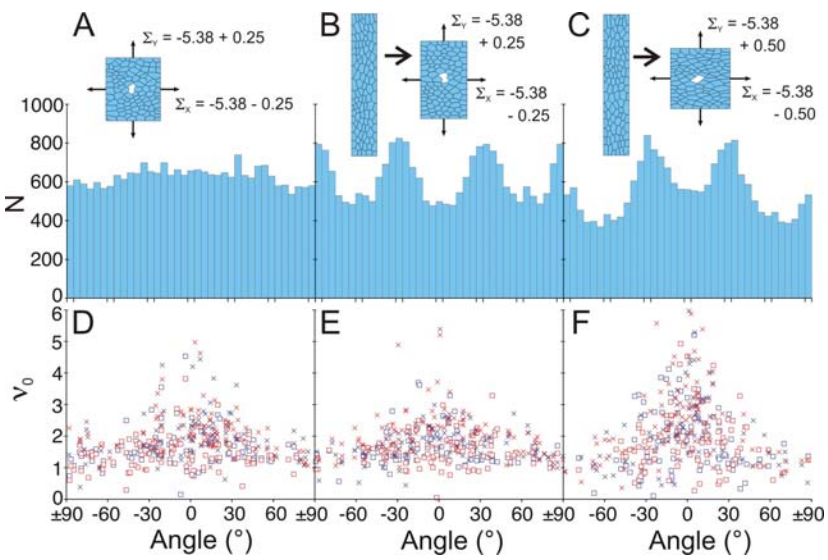

FIGURE S2. Dependence of initial recoil velocity on direction under anisotropic external stress. **(A-C)** Histograms of cell-edge orientations. The external stresses are as shown for the sample cell patches. Note that $\Sigma < 0$ implies cell edges that are under compression. For (B,C), the cell patch was previously stretched in the vertical direction. **(D-F)** Initial recoil velocities versus direction for cell-edge (□) and cell-center (×) wounds. For cell-edge wounds, the tracked direction was always parallel to the ablated edge.

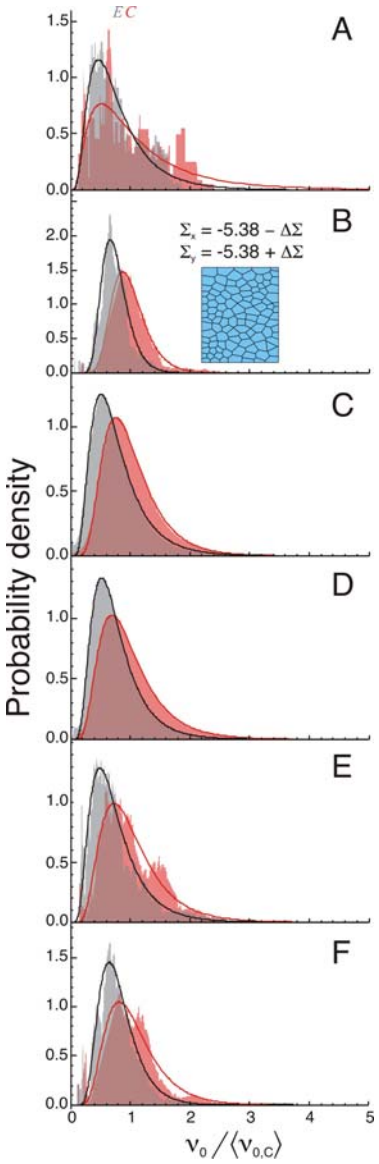

FIGURE S3. Comparison of the ν_0-distributions for experiments **(A)** and simulations **(B-F)** for late dorsal closure when $\Sigma < 0$, i.e. cell edges are under compression: **(B)** best-matching uniform simulations; **(C)** simulations with inter-embryo lognormal variations in $|\Sigma|$; **(D)** simulations with inter-embryo lognormal variations in all |force/viscosity| ratios; **(E)** simulations with intra-embryo lognormal variations in viscosity; **(F)** non-equilibrium simulations with intra-embryo lognormal variations in the interfacial tension magnitude. Cell-center wounds are in red, cell-edge wounds in grey. $\langle \nu_{0,C} \rangle$ and $\langle \nu_{0,E} \rangle$, are marked by the red *C* and grey *E* respectively. The sample cell patch in (B) shows the cell geometry after equilibration at the noted stress $\Sigma_{x,y}$.

Table S1. Viscoelastic parameters used in the simulations presented in Figure 7.

Viscoelastic rods along cell edges only

Fit to:	R^2	$\Phi\Psi_M$	$\Phi\xi_M$	$\Phi\Psi_K$	$\Phi\xi_K$
mean – st. dev.	.999242	1750	767	27.5	0
mean	.999653	750	349	10.0	0
mean + st. dev.	.999447	500	174	6.25	0

Viscoelastic rods as a pre-stressed intracellular mesh

Fit to:	R^2	Σ_{mesh}	$\Phi\Psi_M$	$\Phi\xi_M$	$\Phi\Psi_K$	$\Phi\xi_K$
mean – st. dev.	.999256	3.27	1.00	0.506	2.50×10^{-3}	1.74×10^{-2}
mean	.999651	3.16	0.625	0.251	1.25×10^{-3}	1.74×10^{-2}
mean + st. dev.	.999474	2.90	0.375	0.293	1.25×10^{-3}	1.74×10^{-2}
Double-wound simulation		3.75	0	0	0.497	1.34×10^{-2}